

## (3*R*,4*S*)-4-(4-Fluorophenyl)-3-hydroxymethyl-1-methylpiperidine: Conformation and Structure Monitoring by Vibrational Circular Dichroism

Petr Bouř,<sup>\*,†,§</sup> Hana Navrátilová,<sup>||</sup> Vladimír Setnička,<sup>†</sup> Marie Urbanová,<sup>‡</sup> and Karel Volka<sup>†</sup>

Department of Analytical Chemistry and Department of Physics and Measurement, Institute of Chemical Technology, Technická 5, 166 28 Praha 6, Czech Republic; Institute of Organic Chemistry and Biochemistry, Academy of Sciences of the Czech Republic, Flemingovo nám. 2, 16610, Praha 6, Czech Republic; and Department of Organic Chemistry, Faculty of Science, Masaryk University, Kotlářská 2, 611 37 Brno, Czech Republic

bour@uochb.cas.cz

Received September 6, 2001

Absorption and vibrational circular dichroism (VCD) spectra of the title compound, a common intermediate in synthesis of many pharmaceuticals, were measured and analyzed in order to determine its absolute configuration and prevailing conformations. The analysis was combined with a systematic conformer search based on relative energies as well as with comparison of experimental and computed NMR shifts. The spectra were interpreted on the basis of ab initio simulations. The results indicate that the compound adopts exclusively a chair conformation of the piperidine ring with all the fluorophenyl, hydroxymethyl, and methyl substituents attached in equatorial positions. A limited rotation of the hydroxymethyl group is most consistent with the observed VCD pattern. VCD parameters were found significantly more sensitive to conformational changes than absorption or NMR. Concentration dependence of the absorption spectra indicated aggregation in concentrated solutions, but involved hydrogen bonds probably do not influence molecular conformation.

### Introduction

From the beginning, circular dichroism has been acknowledged as an extremely sensitive probe of subtle changes in molecular structure.<sup>1</sup> For example, electronic circular dichroism (ECD) reflects peptide or nucleic acid conformations more reliably than just absorption spectroscopy and is the preferred analytical method today.<sup>2</sup> However, over-sensitivity to the molecular environment and a lack of nonempirical interpretational tools somewhat delayed applications of the technique in general chemistry.<sup>3</sup> These obstacles were overcome for vibrational circular dichroism (VCD) spectra<sup>4</sup> that are less sensitive to solvent and richer in readable structural information. Perhaps the most significant advantage of VCD is its good theoretical background, enabling one to decipher the spectral information and assign intensity features to functional groups independently of empirical knowledge. Traditionally, such studies have been restricted to rather smaller and simpler systems, because of limited accuracy of the theory.<sup>5–7</sup> Remarkable improvements of the experimental and computational techniques led to applica-

tions for more complex molecules, including peptides and nucleic acids.<sup>8–10</sup> Lately, the Food and Drug Administration recognized the technique as a stereochemistry proofing tool. However, interpretations of spectra of flexible systems still remain a challenge for VCD spectroscopy. In particular, the study of (3*R*,4*S*)-4-(4-fluorophenyl)-3-hydroxymethyl-1-methylpiperidine (referred to as MP, see Figure 1 for the structure) presented here reveals many interesting limits, advantages, and restrictions of VCD spectroscopy and computational chemistry.

The enantiomer with absolute configuration (3*S*,4*R*) is a key intermediate in the synthetic pathway to paroxetine while the (3*R*,4*S*) enantiomer<sup>11</sup> with a phenyl group instead of 4-fluorophenyl is used in the synthesis of femoxetine. Both pharmaceuticals are selective serotonin (5HT) reuptake inhibitors.<sup>12,13</sup> Recently, enantioselective synthetic routes to the chiral *trans*-4-aryl-3-substituted-piperidine molecular skeleton were discovered.<sup>14</sup> The

\* To whom correspondence should be addressed. Fax (420-2)-2431-0503.

<sup>†</sup> Department of Analytical Chemistry, Institute of Chemical Technology.

<sup>‡</sup> Department of Physics and Measurement, Institute of Chemical Technology.

<sup>§</sup> Academy of Sciences of the Czech Republic.

<sup>||</sup> Masaryk University.

(1) Charney, E. *The Molecular Basis of Optical Activity*, John Wiley & Sons: New York, 1979.

(2) Johnson, W. C., Jr. *Annu. Rev. Biophys. Biophys. Chem.* **1988**, *17*, 145–166.

(3) Furche, F.; Ahlrichs, R.; Wachsmann, C.; Weber, E.; Sobanski, A.; Vögtle, F.; Grimme, S. *J. Am. Chem. Soc.* **2000**, *122*, 1717–1724.

(4) Barron, L. D. *Molecular Light Scattering and Optical Activity*, Cambridge University Press: Cambridge, 1982.

(5) Black, T. M.; Bose, P. K.; Polavarapu, P. L.; Barron, L. D.; Hecht, L. *J. Am. Chem. Soc.* **1990**, *112*, 1479–1489.

(6) Tam, C. N.; Bouř, P.; Keiderling, T. A. *J. Am. Chem. Soc.* **1996**, *118*, 10285–10293.

(7) Bouř, P.; McCann, J.; Wieser, H. *J. Phys. Chem. A* **1998**, *102*, 102–110.

(8) Silva, R. A. G. D.; Kubelka, J.; Bouř, P.; Decatur, S. M.; Keiderling, T. A. *Proc. Natl. Acad. Sci. U.S.A.* **2000**, *97* (15), 8318–8323. Keiderling, T. A. In *Biomolecular Structure and Dynamics*; NATO ASI Series, Series E: Applied Sciences Vol. 342, Vergoten, G., Theophanides, T., Eds.; Kluwer Academic Publishers: Dordrecht, 1997; pp 299–317.

(10) Birke, S. S.; Diem, M. *Biophys. J.* **1995**, *68*, 1045–1049.

(11) Jones, P. G.; Kennard, O.; Horn, A. S. *Acta Crystallogr.* **1979**, *B35*, 1732–1735.

(12) Mathis, C. A.; Gerdes, J. M.; Enas, J. D.; Whitney, J. M.; Taylor, S. E.; Zhang, Y.; McKenna, D. J.; Havlik, S.; Peroutka, S. J. *J. Pharm. Pharmacol.* **1992**, *44*, 801–805.

(13) Engelstoft, M.; Hansen, J. B. *Acta Chem. Scand.* **1996**, *50*, 164–169.

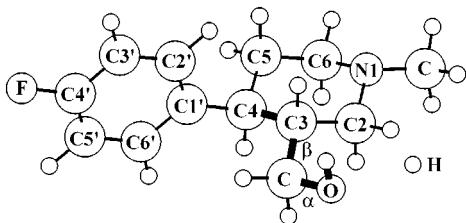


**Figure 1.** Structure and characteristic torsion angles ( $\alpha$ ,  $\beta$ ) for the lowest-energy conformation (I) of (3*R*,4*S*)-4-(4-fluorophenyl)-3-hydroxymethyl-1-methylpiperidine.

neurochemical activity of these compounds depends on absolute configuration, enantiometric purity, and presumably on molecular conformation,<sup>15</sup> which can be all conveniently monitored by VCD. An NMR analysis of enantiomer mixtures will be published in a separate study. In this work we wanted to confirm the absolute configuration of MP (supposed to be (3*R*,4*S*)) and find its conformations in solution. Note that the 5HT (anti-depressive) drugs are marketed as single enantiomers. To the best of our knowledge, no data were published on determining or confirming the absolute configuration of paroxetine or its chiral precursors.

We also hope that this study can contribute to the general methodology of VCD spectroscopy and enhance its applications for pharmaceutically important compounds. The technique became commercially available<sup>16</sup> at the end of the past decade as the sensitivity and stability of the spectrometers increased. Spectra, not only of small molecules but also of biopolymers and other macromolecular systems, can be interpreted on the basis of *ab initio* simulations. As a standard, the Stephens magnetic field perturbation (MFP) theory<sup>17,18</sup> is used for calculation of VCD intensities, available for example in the Gaussian program package<sup>19</sup> implemented within the harmonic approximation of molecular force field. Other theories, such as vibronic coupling theory (VCT)<sup>20</sup> or the excitation scheme (EXC, SOS),<sup>21</sup> provided comparative results, but their computer implementations are not so convenient as for MFP. The methods of the density functional theory (DFT)<sup>22</sup> enabled computations of force constants and harmonic vibrational frequencies for large

systems, the size of which can be further extended by the atomic tensor transfer techniques.<sup>23</sup> However, the methods become less accurate as the dimensions of the systems grow; solvent and anharmonic interactions are involved and studied molecules become more flexible. Thus, we consider it useful to study medium-sized systems for which the theory can be thoroughly tested and future needs of the interpretational apparatus assessed. For the MP molecule, the interaction with the solvent is limited and accurate *ab initio* methods can be consistently applied. Because of many degrees of conformational freedom, the spectral analysis is more complicated than for similar models studied previously, but can also bring more information providing the simulations are accurate enough. Finally, we regard the symbiotic analysis by complementary techniques (in this case *ab initio* modeling, and absorption, VCD, and NMR spectroscopy) as an important development.

## Experimental Section

Enantiomerically pure (100% enantiomeric excess) and enriched (65.2% ee for the opposite enantiomer) samples of MP were kind gifts of Synthron BV, Netherlands. A higher enantiomeric excess for the second enantiomer (96%) was obtained by the reverse enrichment procedure.<sup>24</sup> Proton and carbon-13 NMR spectra were obtained at 303 K in CDCl<sub>3</sub> on a Bruker Avance DRX 500 working at 500.12 MHz for proton and at 125.76 MHz for carbon-13 signal recording, respectively.

VCD and infrared absorption spectra were recorded simultaneously with spectral resolution of 4 cm<sup>-1</sup> on an FTIR IFS 66/S spectrometer equipped with the VCD/IRRAS module PMA 37 (Bruker, Germany). A low-pass filter (<1800 cm<sup>-1</sup>), BaF<sub>2</sub> polarizer, ZnSe modulator (Hinds Instruments) oscillating at the frequency of 50 kHz, and MCT (Infrared Associates) detector were used. Experimental setup and instrument performance were described in detail elsewhere.<sup>25</sup> Samples were dissolved (0.64 mol L<sup>-1</sup>) in CCl<sub>4</sub> (>99.9%, Uvasol, Merck) and CDCl<sub>3</sub> (>99%, Uvasol, Merck) and placed in a demountable KBr cell (A145, Bruker, Germany) separated with a 50  $\mu$ m Teflon spacer. VCD spectra were obtained as an average of three blocks of 3380 scans. OPUS 3.0.2 software (Bruker, Germany) was used for the spectra processing.

## Computations

With the aid of the Spartan<sup>26</sup> program, lowest-energy conformations of MP were found using a systematic search procedure and molecular mechanics (MM) MMFF<sup>27</sup> force field. Obtained structures were reoptimized at the AM1<sup>28</sup> molecular orbital level with the same program. Then program Gaussian was used in order to assess the relative energies at the more advanced HF/6-31G, HF/6-31+G\*\*, Becke3LYP<sup>29,30</sup> (B3L)/6-31+G\*\*, and Becke-Perdew-Wang<sup>29,31</sup> (BPW91)/6-31+G\*\* levels. Additionally, solvent-adjusted energies were obtained at the HF/6-31G and HF/6-31+G\*\* levels with the COSMO solvent model<sup>32,33</sup> implemented in the Turbomole<sup>34,35</sup> program.

(14) Amat, M.; Hidalgo, J.; Bosch, J. *Tetrahedron: Asymmetry* **1996**, 7, 1591–1594.

(15) Jones, P. G.; Kennard, O. *Acta Crystallogr., Sect. B* **1979**, 35, 1732–1735.

(16) For example, BioTools, Inc., or Bruker Optics, Inc.

(17) Stephens, P. J. *J. Phys. Chem.* **1985**, 89, 748–752.

(18) Devlin, F. J.; Stephens, P. J.; Cheeseman, J. R.; Frisch, M. J. *J. Phys. Chem. A* **1997**, 101, 9912–9924.

(19) Frisch, M. J.; Trucks, G. W.; Schlegel, H. B.; Scuseria, G. E.; Robb, M. A.; Cheeseman, J. R.; Zakrzewski, V. G.; Montgomery, J. A.; Stratmann, R. E.; Burant, J. C.; Dapprich, S.; Millam, J. M.; Daniels, A. D.; Kudin, K. N.; Strain, M. C.; Farkas, O.; Tomasi, J.; Barone, V.; Cossi, M.; Cammi, R.; Mennucci, B.; Pomelli, C.; Adamo, C.; Clifford, S.; Ochterski, J.; Petersson, G. A.; Ayala, P. Y.; Cui, Q.; Morokuma, K.; Malick, D. K.; Rabuck, A. D.; Raghavachari, K.; Foresman, J. B.; Cioslowski, J.; Ortiz, J. V.; Stefanov, B. B.; Liu, G.; Liashenko, A.; Piskorz, P.; Komaromi, I.; Gomperts, R.; Martin, R. L.; Fox, D. J.; Keith, T.; Al-Laham, M. A.; Peng, C. Y.; Nanayakkara, A.; Gonzalez, C.; Challacombe, M.; Gill, P. M. W.; Johnson, B. G.; Chen, W.; Wong, M. W.; Andres, J. L.; Head-Gordon, M.; Replogle, E. S.; Pople, J. A. *Gaussian 98, revisions A.3 and A.7*; Gaussian, Inc.: Pittsburgh, PA, 1998.

(20) Nafie, L. A.; Freedman, T. B. *J. Chem. Phys.* **1983**, 78, 7108–7116.

(21) Bouř, P.; McCann, J.; Wieser, H. *J. Chem. Phys.* **1998**, 108, 8782–8789.

(22) Laird, B. B.; Ross, R. B.; Ziegler, T., Eds. *Chemical Applications of Density-Functional Theory*; ACS Symposium Series 629, American Chemical Society: Washington, D.C., 1996.

(23) Bouř, P.; Sopková, J.; Bednářová, L.; Maloň, P.; Keiderling, T. A. *J. Comput. Chem.* **1997**, 18, 646–659.

(24) Navrátilová, H. Ph.D. Thesis, Faculty of Science, Masaryk University: Brno, Czech Republic, 2001.

(25) Urbanová, M.; Setnička, V.; Volka, K. *Chirality* **2000**, 12, 199–203.

(26) *PC Spartan Pro 1.0.5*, Wavefunction, Inc.: Irvine, 2000.

(27) Halgren, T. A. *J. Comput. Chem.* **1996**, 17, 490–519.

(28) Dewar, M. J. S.; Reynolds, C. H. *J. Comput. Chem.* **1986**, 2, 140–143.

(29) Becke, A. D. *J. Chem. Phys.* **1993**, 98, 5648–5652.

(30) Lee, C.; Yang, W.; Parr, R. G. *Phys. Rev. B* **1988**, 37, 785–789.

(31) Perdew, J. P.; Wang, Y. *Phys. Rev. B* **1992**, 45, 13244–13249.

**Table 1. Calculated Relative Energies (kcal/mol) of 15 Conformers**

	MM	AM1	HF/6-31G	HF/6-31+G**	HF/6-31G COSMO	HF/6-31+G** COSMO	B3L/6-31+G**	BPW91/6-31+G**
XV	6.9	3.9	6.0	11.2	9.9	11.1	10.9	10.7
XIV	7.5	4.1	6.3	7.4	7.8	8.7	7.2	7.2
XIII	3.2	4.7	4.5	5.7	6.2	5.7	5.2	5.4
XII	6.8	3.7	4.2	5.1	5.2	5.7	5.2	5.2
XI	2.0	4.5	3.5	4.4	4.9	5.3	4.3	4.5
X	2.9	0.3	2.6	3.6	2.7	3.5	3.7	3.7
IX	4.6	1.7	3.0	4.7	4.2	6.1	3.6	2.9
VIII	3.6	- <sup>a</sup>	3.8	2.8	2.0	1.6	2.7	2.8
VII	1.6	3.0	2.5	3.8	3.6	5.3	2.1	1.5
VI	1.8	0.3	0.2	0.9	0.7	0.5	0.8	0.8
V	1.2	0.5	0.2	0.3	0.7	0.8	0.5	0.5
IV	2.2	0.4	1.6	1.0	2.0	1.6	0.6	0.5
III	-0.9	2.3	-0.8	-0.6	0.4	0.2	0.0	0.4
II	-0.1	1.9	-0.3	-0.3	0.1	-0.2	-0.1	0.2
I	0.0	0.0	0.0	0.0	0.0	0.0	0.0	0.0

<sup>a</sup> Local minimum does not exist.

**Table 2. Characteristic Torsion Angles Computed for the Most Stable Conformers<sup>a</sup>**

conformation	phenyl position	methyl position	piperidine ring	MM		BPW91/6-31+G**	
				$\alpha$	$\beta$	$\alpha$	$\beta$
XV	E	A	boat	-174	-178	178	-179
XIV	A	E	boat	178	-178	180	-178
XIII	A	E	chair	-171	-168	-167	-170
XII	E	E	boat	-171	-172	-177	-171
XI	A	E	chair	-178	-65	173	-63
X	E	A	chair	178	-177	178	-175
IX	E	E	boat, OH bridge	41	61	53	53
VIII	E	E	chair	176	-75	168	-84
VII	A	E	chair, OH bridge	43	60	35	66
VI	E	E	chair	-85	-176	-80	-174
V	E	E	chair	-88	60	-83	58
IV	E	E	chair	67	-80	60	-79
III	E	E	chair	180	63	-175	61
II	E	E	chair	172	-177	178	-176
I	E	E	chair	61	180	70	-177

<sup>a</sup> Letters E/A denote equatorial/axial positions. Torsion angles  $\alpha$  and  $\beta$  are defined in Figure 1.

For all the methods, the molecule was fully relaxed and optimized without any constraints. The relative permittivity was set to 4.9, to mimic the CDCl<sub>3</sub> solvent. Finally, vibrational frequencies and absorption and VCD intensities were obtained by Gaussian at the BPW91/6-31+G\*\* level, and corresponding spectra were simulated using a Lorentzian bandwidth of 5 cm<sup>-1</sup>. The BPW91 DFT functional was selected since it provided excellent results for VCD simulations in previous work.<sup>7,36</sup> On the basis of common experience,<sup>37,38</sup> we consider the inclusion of the diffuse functions (+) desirable for accurate prediction of spectral intensities. The simulation of VCD spectra included seven lowest-energy conformers, since a significant presence of the higher-energy conformations appears improbable under our experimental conditions. The fast multipole method (FMM)<sup>39</sup> implemented in Gaussian was used in order to speed up the computations. At the same BPW91/6-31+G\*\* level nuclear magnetic shielding con-

stants were calculated for 15 conformers, using the default CP/GIAO<sup>40</sup> method.

## Results

Computed relative energies (with respect to the lowest BPW91/6-31+G\*\* conformer) of 15 lowest-energy conformations out of about 100 obtained by the systematic search are given in Table 1. Corresponding characteristic geometry parameters are summarized in Table 2. Rather surprisingly, relative AM1 energies agree with the ab initio values less than for the simpler MM method. Six lowest-energy conformations differ in energies by less than 1 kcal/mol if calculated by the two last most-advanced methods. Inclusion of the solvent via the COSMO model changes the energies by 0.1–3.9 kcal/mol, thus changing the ordering of several conformations. For the vacuum HF method, the change of basis from 6-31G to 6-31+G\*\* led to an exceptionally large increase of energy for the conformer XV (by 5.2 kcal/mol), but had otherwise minor effect on conformer ordering.

Experimental chemical shifts are summarized in Table 3. The NMR spectra were measured in CDCl<sub>3</sub>. Control experiments showed little variance of the experimental shifts if C<sub>6</sub>D<sub>6</sub> solvent or a racemic sample was used, which we consider negligible for the comparison with the theoretical values. Table 4 lists mean square root devia-

(32) Klamt, A.; Schürmann, G. *J. Chem. Soc., Perkin Trans. 2* **1993**, 2, 799–805.

(33) Klamt, A. *J. Phys. Chem.* **1995**, *99*, 2224–2235.

(34) Klamt, A. in *The Encyclopedia of Computational Chemistry*; Schleyer, P. v. R., Allinger, N. L., Clark, T., Gasteiger, J., Kollman, P. A., Schaefer, H. F., III, and Schreiner, P. R., Eds. John Wiley & Sons: Chichester, 1998; pp 604–615.

(35) *Turbomole 5*, University of Karlsruhe, 1999.

(36) Bouř, P.; McCann, J.; Wieser, H. *J. Phys. Chem. A* **1997**, *101*, 9783–9790.

(37) Rauk, A.; Yang, D. *J. Phys. Chem.* **1992**, *96*, 473–446.

(38) Florián, J.; Šponer, J.; Warshel, A. *J. Phys. Chem. B* **1999**, *103*, 884–892.

(39) Burant, J. C.; Strain, M. C.; Scuseria, G. E.; Frisch, M. J. *Chem. Phys. Lett.* **1996**, *258*, 45–52.

(40) Wolinski, K.; Hinton, J. F.; Pulay, P. *J. Am. Chem. Soc.* **1990**, *112*, 8251–8260.

**Table 3. Experimental Proton and Carbon Chemical Shifts**

moiety	$\delta_{\text{H}}$ (ppm)	$\delta_{\text{C}}$ (ppm)
CH <sub>3</sub>	2.27	46.41
2	3.16, 1.87	59.54
3	1.92	44.21
4	2.25	43.61
5	1.75, 1.72	34.29
6	2.86, 1.98	56.15
CH <sub>2</sub> O	3.33, 3.16	63.12
OH	3.87	
1'		139.96
2'	7.15	128.81
3'	6.94	115.28
4'		161.42
5'	6.94	115.28
6'	7.15	128.81

tions from the computed shifts as calculated for the whole set of 15 lowest-energy conformations. Relative TMS shifts were compared,  $\sigma_{\text{rel}} = \sigma_{\text{TMS}} - \sigma_{\text{absolute}}$ , where the TMS isotropic shielding ( $\sigma_{\text{TMS}}$ ) was calculated as 31.35 and 191.30 ppm for hydrogen and carbon-13 atoms, respectively, at the same BPW91/6-31+G\*\* level. The hydroxyl group was excluded from the comparison, because of its polarity and anomalously strong interaction with the environment, supposedly via hydrogen bridges. A set of favorite conformations (I–VI and VIII) can be identified with the error smaller than 0.32 ppm, while the rest exhibits deviations bigger than 0.5 ppm. This can be also seen if the differences between calculated and observed shifts are plotted for all hydrogen atoms, as in Figure 2. Chemical shifts for carbons (<sup>13</sup>C) are rather conformation-independent and, although higher in absolute values, the mean deviations among experimental and theoretical data are relatively small, typically about 10%.

The level of the overall agreement between experimental and calculated frequencies and absorption intensities in the entire frequency range can be seen in Figure 3. A dissolved solution (0.064 mol/L, in CCl<sub>4</sub>) was used in order to minimize intermolecular hydrogen bridging. Calculated spectra (BPW91/6-31+G\*\*, conformer I) are plotted in the same *x* and *y* scales, without additional scaling. Computed frequencies are by about 2.5% higher than experimental ones for the O–H and C–H stretching vibrations, while even closer match was achieved for most modes in the mid-IR region, as follows from the detailed assignment in Table 5. Detailed assignment for the mid-IR region is presented in Table 6 together with VCD spectral intensities for conformations I–VII. The assignment of vibrational modes is based on a visual inspection of the normal mode displacements as well as comparison of relative atomic kinetic energies. The error in Table 6 was defined as the number of obvious disagreements between measured and calculated VCD signs. In Figure 4 simulated absorption spectra in the mid-IR region are plotted for the seven conformations (I–VII), to illustrate the differences qualitatively. Also, the absorption spectrum of the best conformation of the (3*R*,4*R*)-isomer (top trace in the figure) is clearly distinguishable from most conformations of the (3*R*,4*S*)-isomer. We propose to model the measured spectrum as a sum of the conformers I, II, III, and VI. Indeed, as can be seen in Figure 4, such a sum matches well the main intensity features present in the experimental spectrum. Finally, we present a similar comparison of VCD spectra in Figure 5. Similarly, as for the absorption, the spectrum of the (*R*,*R*)-isomer

does not match the experiment. We find it obvious that the data corresponds to the desired enantiomer, and the conformational dependence for (*R*,*R*) was not studied further because of computational limits and a lack of experimental data for this isomer. On the other hand, simulated conformational dependence of the VCD spectra for the (*R*,*S*) isomer allows us to select the most probable conformations. Their sum very well approximates the measured spectrum, as can be seen in the lower part of Figure 5.

To assess possible aggregation via hydrogen bonds, energies of three MP dimers (with the acidic hydrogen bound to F, O, and N atoms) were estimated at the BPW91/6-31+G\*\* level, as summarized in Table 7. Conformer II was considered in the complexes, with  $\alpha \sim 180^\circ$ , cf. Table 2, where the OH groups are presumably most prone to formation of the hydrogen bonds. Starting geometries were constructed with an approximate linear arrangement of the hydrogen bond atoms (O–H...X). The hydrogen binding to the nitrogen atom appears strongest with the stabilization energy for the dimer of 6.5 kcal/mol and leads to the biggest change of the NMR shift.

## Discussion

**Energies and NMR Spectra.** As follows from the relative energies listed in Table 1, under the experimental conditions for VCD and NMR spectra measurement ( $kT \sim 0.6$  kcal/mol), the molecule exhibits almost exclusively the chair conformation of the six-membered ring with the fluorophenyl and methyl residues attached in equatorial positions. The inclusion of the solvent does not change this preference. This is in agreement with X-ray data for crystals of similar systems.<sup>41</sup> Since the expected error of the calculations is comparable with the Boltzmann quantum, detailed conformer distribution in the sample cannot be assessed solely on the basis of energy computation. The inclusion of the solvent slightly smoothes differences between relative energies of conformers I–VI, but significantly less than for more polar systems investigated previously.<sup>42</sup> Presumably, dynamic entropy factors that could not be included in our modeling can lower the energy differences even more. The increase of the basis size (from 6-31G to 6-31+G\*\* for the HF method) does not have a decisive role for the conformer ordering.

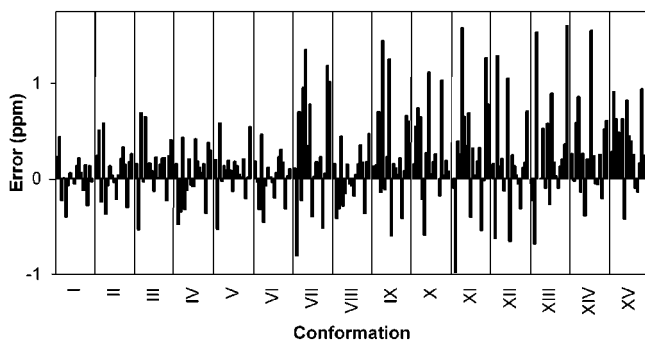
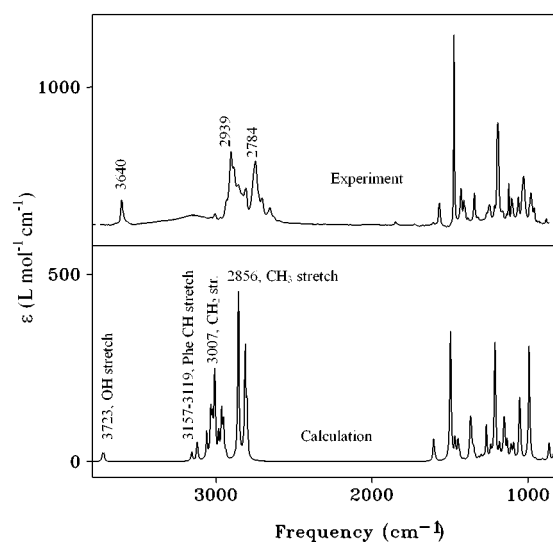
Although a direct comparison of computed and experimental shifts can be obscured by a time and conformational averaging, comparison for a larger set of atoms should provide a more reliable indication of allowed conformations. The dependence of NMR shielding on conformations appears as a promising tool for conformational studies, and it is rare in previous literature dealing predominantly with modeling of rigid molecules. For our case, the calculation nicely complements the energy studies. For example, the bridged-conformation (VII) with a rather low energy of 1.5 kcal/mol can be excluded from the set of most populated conformations, because of the discrepancy between computed and measured hydrogen NMR shifts. On the other hand, reasonable shifts are predicted for conformer VIII, but its relative energy (2.8 kcal/mol, see Table 1) is high, and its presence in the sample not probable.

(41) Yamada, S.; Ichikawa, M. *Tetrahedron Lett.* **1999**, *40*, 4231–4234.

(42) Bouř, P.; Král, V. *Collect. Czech. Chem. Commun.* **2000**, *65* (5), 631–643.

**Table 4. Mean Deviations between Calculated and Experimental Chemical Shifts (ppm) for MP Conformers**

conformer	I	II	III	IV	V	VI	VII	VIII	IX	X	XI	XII	XIII	XIV	XV
	Hydrogens (without OH):														
mean deviation	0.20	0.28	0.32	0.28	0.26	0.23	0.67	0.27	0.58	0.50	0.67	0.51	0.65	0.52	0.51
	Carbons														
mean deviation	8.86	8.62	8.60	9.23	8.41	9.21	8.67	9.37	8.73	8.74	9.36	8.61	8.87	9.14	8.74

**Figure 2.** Differences between computed and experimental NMR hydrogen shifts (17 atoms included, without OH, see Figure 1) for 15 conformers.**Figure 3.** Calculated (conformation I, BPW91/6-31+G\*\*) and experimental (0.032 mol/L solution in CCl<sub>4</sub>) absorption spectra. See Tables 5 and 6 for the assignments in the mid-IR region.

Calculated NMR shifts for conformations III and V exhibit slight positive systematic deviations from the experiment (cf. Figure 2), but these are less obvious and comparable with the overall error of the modeling. On the contrary, all of the higher-energy conformers (IX–XV) consistently exhibit unrealistic values of calculated shifts. Hydrogen shielding is clearly more sensitive than carbon shifts, which can be explained by the lack of core electrons uninfluenced by the conformational changes.

As can be deduced from Table 7, the anomalous NMR shift of the OH hydrogen can be explained by the hydrogen binding and aggregation. Indeed, the shift of 0.02 ppm calculated for the monomer (conformer II) increases up to 6.14 ppm for the last complex [MP-OH⋯N-MP]. Supposedly both the OH⋯O and OH⋯N type hydrogen binding occurs in the sample, the exact ratio of which is difficult to judge on the basis of the energy calculations because of the influence of solvent and other factors involved. Nevertheless, the indication that the molecule forms strong intermolecular complexes is in

**Table 5. Calculated Harmonic Frequencies and Assignment to Observed Bands**

mode <sup>a</sup>	calcd	exp	mode	calcd	exp
19	1603.7	1600	43	1212.9	1226
20	1594.1		44	1208.1	
21	1496.4	1510	45	1182.3	1213
22	1467.9	1470	46	1166.5	1175
23	1466.0	1470	47	1154.9	1159
24	1462.0	1449	48	1149.7	
25	1448.4		49	1132.8	1134
26	1447.1		50	1108.4	1107
27	1437.7	1438	51	1096.4	1099
28	1416.3	1428	52	1091.7	1085
29	1408.8	1421	53	1073.2	
30	1369.1	1382	54	1053.7	1074
31	1362.2		55	1052.4	1062
32	1361.0		56	1048.1	1022–1016
33	1349.8		57	1001.2	996
34	1339.1	1355	58	992.3	
35	1331.6		59	984.6	982
36	1315.9	1322	60	951.4	
37	1299.9	1301	61	931.3	
38	1290.8		62	918.6	
39	1286.3		63	904.7	920
40	1271.4		64	865.9	
41	1266.8	1281	65	863.2	880
42	1239.2	1249	66	829.8	

<sup>a</sup> Mode numbering corresponds to the total of  $3N - 6 = 96$  vibrational modes, starting with the O–H stretching. Calculated harmonic frequencies with the BPW91/6-31+G\*\* force field for conformer I are given.

accord with the concentration dependence of the absorption spectra mentioned below.

**Absorption and VCD Spectra.** We observed an excellent agreement between calculated absorption frequencies and intensities, as presented in Figures 3 and 4 and Table 5. The computed N–H and C–H stretching frequencies are by about 2–2.5% higher than experimental, which can be partially attributed to anharmonic forces and the influence of the solvent not included in the calculation. In the mid-IR region the BPW91 functional provides a very good model of vibrational frequencies, with an error typically less than 1%, as was found for similar systems previously.<sup>7,21,35,36</sup> The discrepancies in the lowest-frequency region (900–1100 cm<sup>-1</sup>) between experimental and computed intensities for the first (I) conformer strongly suggest a presence of more conformations. Indeed, as shown in Figure 4, conformational flexibility leads to the same band broadening as observed experimentally in this region.

The (*R,R*)-isomer exhibits some common features with the experimental spectra, namely in the higher-frequency region (cf. Figure 4). However, the split peak calculated for the (*R,R*) form at about 1360 cm<sup>-1</sup>, the distinct three-peak pattern around 1150 cm<sup>-1</sup>, and the high absorption signals at 1018 and 991 cm<sup>-1</sup> do not match experimental intensities. These can be better modeled with lower-energy conformations of the (*R,S*)-isomer, which, in other words, confirms that the synthesis provided the desired product.

A greater variance with respect to conformational changes can be observed in VCD intensities, as can be

**Table 6. Calculated Rotational Strengths ( $10^{-8}$  Debye<sup>2</sup>) and Mode Assignment**

mode	I	II	III	IV	V	VI	VII	exp	remark
19	-1	0	-2	0	-2	-1	0	-	phenyl deformation (C=C stretch)
20	-2	-3	0	-2	-4	-3	1	-	<i>b</i>
21	0	-1	2	0	3	0	5	+	<i>b</i>
22	1	-14	0	-2	2	0	4	-	C-H bend, aliphatic
23	-4	2	2	2	-3	-1	-11	-	<i>b</i>
24	-12	-4	-3	4	5	-3	-26	-	C-H bend, aliphatic and OH
25	2	4	-5	-5	-2	-5	-22	-	C-H bend, aliphatic
26	-6	-7	3	2	1	0	5	-	<i>b</i>
27	8	8	9	6	8	8	2	+	<i>b</i>
28	0	0	-1	0	0	0	27	+	CH <sub>3</sub> umbrella mode
29	-1	-1	-1	0	-2	-2	-1	-	C-H bend, aliphatic and phenyl
30	-44	-18	-6	2	7	-66	1	-	C-H, OH bend
31	3	-23	0	3	0	30	3	-	<i>b</i>
32	6	-3	-2	-4	4	9	1	-	<i>b</i>
33	13	12	-18	-31	-4	1	-4	-	CH <sub>2</sub> wagging
34	13	-5	16	10	-8	1	-11	+	<i>b</i>
35	-4	12	10	-33	-10	30	0	-	<i>b</i>
36	27	1	5	6	9	8	-2	+	<i>b</i>
37	9	1	-26	-17	-1	10	-11	-	CH <sub>2</sub> twist + phenyl def.
38	2	29	7	9	11	13	2	-	<i>b</i>
39	22	21	12	-3	-40	-4	31	+	<i>b</i>
40	16	-42	-15	-10	-2	-17	-3	-	CH <sub>2</sub> twist + CH <sub>3</sub> def.
41	-74	14	2	5	-8	-22	-15	-	<i>b</i>
42	2	35	18	21	33	-3	-5	+	C-C(Phenyl) stretch
43	29	87	3	37	50	21	13	+	C-F stretch
44	-1	-73	-6	-28	-6	5	-12	-	skeletal deformation, CH bend
45	-21	30	20	-18	0	4	13	+	skeletal deformation, phenyl
46	-10	-12	-34	-4	7	2	2	-	skeletal deformation
47	0	42	54	39	-16	19	-1	+	<i>b</i>
48	1	2	-12	-12	13	3	-12	-	C-F stretch
49	-6	-50	-2	-23	-4	-43	-3	-	skeletal deformation
50	-10	-7	-9	-12	-12	7	-13	-	<i>b</i>
51	-15	2	32	-12	-2	-14	24	-	<i>b</i>
52	28	-2	-5	6	-13	18	3	+	<i>b</i>
53	2	-15	-8	7	53	2	-43	-	<i>b</i>
54	-67	-12	-47	-44	24	-39	40	-	<i>b</i>
55	31	-21	52	37	-34	8	17	-	skeletal deformation, C-O stretch
56	5	-11	-78	32	-57	31	-52	+	<i>b</i>
57	4	0	-4	-30	-2	22	49	+	phenyl deformation
58	26	-3	13	0	30	-4	7	-	C-O stretch
59	32	7	38	-10	43	-22	7	+	skeletal deformation, C-N stretch
60	-3	2	-7	7	0	8	0	-	skeletal deformation
61	0	0	0	0	-15	0	10	-	phenyl deformation
62	2	2	3	16	0	2	-8	-	out of plane phenyl deformation
63	-2	-3	-7	0	-12	-3	-6	-	skeletal deformation, C-C stretch
64	38	1	0	18	-16	14	-2	-	delocalized deformation
65	-11	58	18	9	24	-17	-22	+	<i>b</i>
66	5	3	62	79	72	6	-18	-	<i>b</i>
Error <sup>a</sup>	6	9	9	14	12	9	12		

<sup>a</sup> Number of sign disagreements between calculated and experimental VCD spectra. <sup>b</sup> Same as above entry.

seen in Figure 5 and Table 6. We realize that analysis of VCD spectra is somewhat influenced by their visual inspection prone to human error, as no universal approaches exist yet. For example, modes can be ordered and compared with experiment according to their energies (as in Table 6) or according to their nature (e.g., grouping locally symmetric and antisymmetric CH<sub>2</sub> bendings). Nevertheless, as follows from trial computations, both analyses lead to similar conclusions for the MP molecule. The errors, as defined in Table 6, suggest conformations I–III and VI as the most compliant with recorded spectra, which is in accord with the energy analysis and also consistent with the NMR prediction. The sum of these four conformations approximates very well the experimental spectrum in Figure 5. Although a weighted average could have been introduced in order to further improve the agreement, we consider it irrelevant in the present state because of the limited accuracy of the available VCD simulation methods.

In accordance with the absorption modeling, the calculation for the lowest-energy conformation (*R,R*)-isomer provides an unrealistic VCD pattern within the entire frequency region (Figure 5). Obviously, because of the limited accuracy of the experiment and the calculations, other analytical techniques are more suitable for accurate estimation of low concentration impurities in the sample.

Closer inspection of the conformations (Table 2) thus reveals the physical significance of the results. The OH group is preferably oriented in the opposite direction to that of the fluorophenyl group ( $\beta$  is close to 180° for conformers I, II, and VI); in this case the hydrogen rotates freely around the CO bond or retains a set of preferred positions ( $\alpha = 70, 178, \text{ and } -80^\circ$ ). Other orientations of the hydroxymethyl group ( $|\beta| \sim 60^\circ$ ) are limited (in our model to conformer III) because of its repulsion by the bulky fluorophenyl group.

**Electrostatic Potential.** A closer inspection of the molecular electrostatic potential reveals that the favorite conformations are also stabilized by electrostatic forces

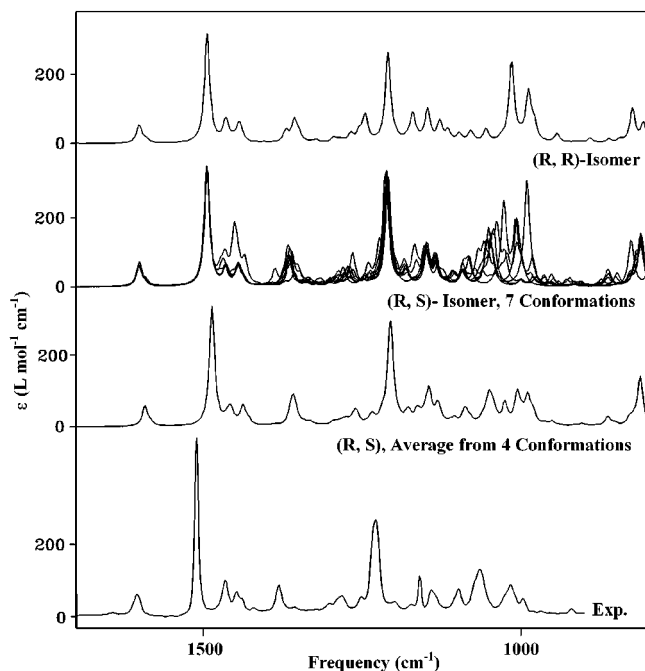


**Figure 4.** Absorption spectra in the mid-IR region. From top to bottom: calculation for the lowest-energy conformation of the (3*R*,4*R*)-isomer, seven lowest-energy conformations (I–VII) and an average spectrum of conformations (I, II, III, and VI) of the (3*R*,4*S*)-isomer, and, finally, the experimental spectrum.

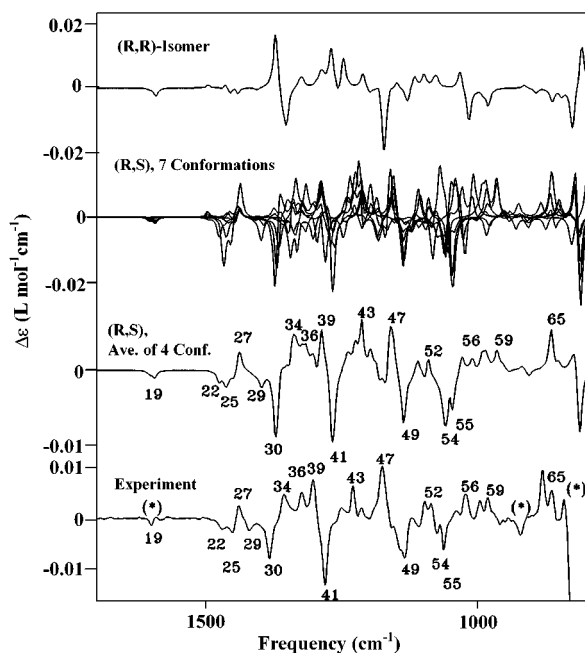


**Figure 5.** VCD spectra in the mid-IR region. From top to bottom: calculated spectra of the lowest-energy conformation of the (3*R*,4*R*)-isomer, seven lowest-energy conformations (I–VII) and an average spectrum of conformations (I, II, III, and VI) of the (3*R*,4*S*)-isomer, and the experiment. The experimental spectrum (CCl<sub>4</sub>, 0.64 mol/L solution) was obtained as a half of the difference of (3*R*,4*S*)- and (3*S*,4*R*)-enantiomer. Asterisk (\*) denotes regions where artifacts may occur in experiment due to the absorption of the solvent.

acting between molecular parts. In Figure 6, the potential is plotted as calculated (HF/6-31G\*\*) for conformer I. Indeed, positively charged hydrogen atoms on the phenyl ring (yellow tint in Figure 6) are attracted by the negative (blue) nitrogen, while the negative charges on nitrogen

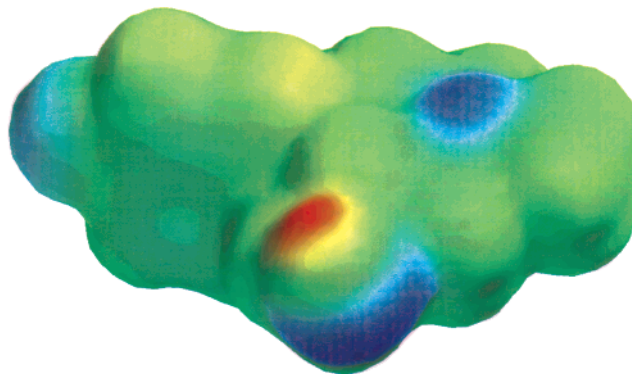


**Figure 6.** Electrostatic potential on the isodensity surface of the MP molecule as calculated for the lowest-energy conformer (I). Blue regions are negative, red are positive.

**Table 7. Complexes of MP: Calculated Stabilization Energies, Hydrogen Bond Lengths, and NMR Isotropic Shift of the Hydroxyl Hydrogen**

complex	$\Delta E$ , kcal/mol	H-bond, Å	$\sigma_{\text{rel}}(\text{H})$ , ppm
MP monomer (conf II)	(0)		0.02
MP–OH $\cdots$ F–MP	0.2	$d(\text{H}\cdots\text{F}) = 2.503$	0.76
MP–OH $\cdots$ OH–MP	3.6	$d(\text{H}\cdots\text{O}) = 1.952$	3.29
MP–OH $\cdots$ N–MP	6.5	$d(\text{H}\cdots\text{N}) = 1.857$	6.14
experimental			3.87

and oxygen atoms are separated by the indifferent aliphatic group as well as by the positively charged hydroxyl hydrogen. The oxygen atom is more exposed to the environment and seems to be more prone to form hydrogen bonds than the nitrogen atom. The proposed free movement of the OH group and the restricted motion of the whole CH<sub>2</sub>OH residue do not change the basic electrostatic pattern.

**VCD Response to Deuteration and Hydrogen Bridges.** To confirm our assignment of vibrational modes, we measured VCD and absorption spectra of the deuterated molecule. Under a standard isotopic exchange with D<sub>2</sub>O, the hydrogen of the OH group was replaced by deuterium. Such a change affected namely the C–H bending modes on the CH<sub>2</sub> group in the vicinity of the OD residuum. Two negative band VCD bands appear in experimental spectra at 1236 and 1259 cm<sup>-1</sup>, which can be faithfully simulated for the sum spectrum of conformers I, II, III, and VI (yielding corresponding bands at 1247 and 1257 cm<sup>-1</sup>, respectively). Thus the assignments in Tables 5 and 6 were partially reconfirmed. Since other changes in the region of recorded frequencies are minor, we did not analyze the spectra of the deuterated species in detail.

A significant dependence of the absorption signal of the O–H stretching vibration on concentration was observed for concentrated solutions. This indicates that also under the experimental conditions for the VCD measurement MP molecules could be linked by hydrogen bridges involving the OH groups. Detailed study about the intermolecular interactions will be also published separately, as it cannot be currently followed by VCD due to its limited sensitivity. Note also that contribution of the OH group affects only a limited region of the measured spectrum (see mode assignments in Table 5). The hydrogen bonding was found both in CDCl<sub>3</sub> and CCl<sub>4</sub> and is also consistent with the anomalous NMR shift found for

the OH group. Nevertheless, the results suggest that the binding does not significantly influence molecular conformation.

### Conclusions

We have confirmed that the synthesis led to the desired absolute configuration of the molecule. A complex analysis based on energy computations, simulation, and measurement of NMR and VCD spectra revealed preferred conformations of the molecule in the sample. The phenyl and methyl groups are attached to the piperidine ring exclusively in equatorial positions, the motion of the

hydroxymethyl group is limited because of the repulsion by the phenyl residue, while the OH residue rotates almost freely in the solution. The *ab initio* modeling provided reasonable estimates of relative conformer energies, NMR, absorption, and VCD spectral parameters.

**Acknowledgment.** The work was supported by grants of the Grant Agency of the Czech Republic (203/01/0031), Grant Agency of the Academy of Sciences (A4055104) and Ministry of Education, Youth, and Sports (CB MSM223400008).

JO016094S